

Acoustophoretic Separation and Electrochemical Impedance Spectroscopic Detection of Microplastics

John K. Goebel¹, Jonathan D. Good², Christopher T. Sharkey², Meghana Manjunath², and Mohammed Abdul Rahman²

¹University of North Carolina at Chapel Hill, Biomedical Engineering

²North Carolina State University, Electrical and Computer Engineering

Abstract—Micro- and nanoplastics (MNPs) are small plastic particles that result from the degradation of larger polymeric chains. MNPs are highly persistent and have been detected in human brain tissue, marine ecosystems, and fetuses. Although the long-term effects of plastics on human health and the environment remain uncertain, they are suspected to be harmful. In this work, we present a scenario in which a common MNP, Polyethylene Terephthalate (PET), is found in water samples with contaminants of crude oil derivatives. By using the differences in acoustic standing-wave behavior and the material characteristics of each contaminant, we will separate the plastic from the oil and determine PET’s composition. We aim to develop a device that uses acoustophoresis (sound waves) and electrochemical impedance spectroscopy (EIS) to separate and detect MNPs in water samples. The proposed device is a three stage microfluidic system fabricated on a lithium chip. It includes an input reservoir, piezoelectric transducers (PZT) for acoustophoretic separation of microplastics from the oil contaminants, PZT’s to separate microplastics from nanoplastics, and a set of EIS electrodes to measure the size distribution, counts, and concentrations of the separated microplastic plastic group. This paper serves as a theoretical reference for the device, using common micro- and nanofabrication techniques such as photolithography, electron beam evaporation, plasma bonding, etc. The device serves as a proof of concept not only for detecting MNPs, but also a cost-effective alternative to conventional microscopic and filtration based detection methods.

Index Terms—acoustophoresis, electrochemical, microfluidics, microplastics, nanoplastics, spectroscopy, transducer, polyethylene terephthalate

I. INTRODUCTION

A. Context

Before you continue reading, take a moment to observe the numerous plastic items in your surroundings. Plastics are inevitable in modern life. In the past 15 years alone, roughly half of all plastics ever produced were manufactured, and production is expected to double or triple by 2050. Excessive use and improper disposal has led to widespread pollution and numerous related environmental and health issues [1]. Some plastics are often called “forever chemicals”, with research indicating that the plastic polymers fragment beyond the micron scale ($<1\ \mu\text{m}$), breaking down further into the nano range at exponentially higher quantities. Determining the exact toxicity of MNPs is an extremely complex problem, as it requires the detailed characterization of each particles properties, composition, and impacts on various morphologies [2].

Assessing the effects of MNPs is beyond this paper’s scope, instead we focus on methods for detecting and separating these particles.

For this study, we investigate MNPs and other contaminants associated with bottled water production. Studies have identified more than 17 different polymers within bottled and tap water [3]. According to a chemical imaging study using stimulated Raman scattering (SRS) microscopy, the concentration of nanoplastics is approximately $2.4 \pm 1.3 \times 10^5$ particles per liter of bottled water, which is about 90% of the total plastics in the water by mass [2]. The remaining 10% (around 3×10^4 particles per liter) are classified as microplastics and are predominantly smaller than $2\ \mu\text{m}$ [2]. Common MNPs in bottled water include PET, polyamide (PA), polypropylene (PP), polyvinyl chloride (PVC), polystyrene (PS), polyethylene (PE), and cellulose (shown in Table I). PET and PE are often used as packaging materials, whereas other polymers such as PA, PP, PS, and PVC are likely introduced into the water before or during production [2].

TABLE I: Common Microplastics in the Water-Bottle Packaging Industry and Their Approximate Densities [4]

Polymer	Density (g/cm ³)	Typical Sources	Notes
PE	0.94	Bags, Packaging, Bottles	Most widely used consumer plastic
PP	0.91	Caps, Straws, Containers	Floats in water
PS	1.05	Foam Packaging, Utensils	Available as foam or rigid forms
PET	1.38	Bottles, Textiles (Polyester)	Common in microfibers

^aValues are approximate; densities vary with polymer grade, additives, and temperature.

By examining differences in density (plastic particle type), quantity, and size, plastic polymers can reveal potential contamination sources during water production and impacts to human health or the environment. According to [2], PET is a major contributor by mass in three popular plastic bottled brands, with particle sizes predominantly in the 1-2 μm range [2].

A secondary contaminant in our ideal water specimen is oil. When oil leaks from spills, it can undergo a series of natural biochemical and physical processes know as “weathering” [5]. Ultimately, the oil breaks down into small bubbles that can remain in the environment for long periods of time. Additionally, metal working fluids used in machining processes generate both airborne and dissolved particles. Particles smaller than $10\ \mu\text{m}$ can remain suspended in an indoor environment for a long time, creating opportunities for inhalation hazards or

cross-contamination with water sources [6]. Crude oil derivatives associated with the bottled water industry could include mineral oil for hydraulic fluid, lubricants (oil/grease) for manufacturing machines, and silicone injection mold release agents. Given these unique scenarios, a complex relationship exists between oil droplet size and various factors such as temperatures effect on oil dispersion into droplets, as well as mixing energy, viscosity, and binding energy of the molecule [7]. To create a controlled condition, we assume oil droplets whose mean size ($10\ \mu\text{m}$) is realistic to real-world settings and reported in previous literature [8].

Existing solutions for both MNPs and oil particles involve filtration, affinity, and density-based separation techniques. Both passive and active microfluidic systems exist for particle sorting including electrical, magnetic, optical and mechanical systems [9]. In terms of MNP water purification, alumina, ceramics, and polycarbonate filters remain highly specific and require continued replacement or cleaning to continue their effectiveness [10]. On the detection side, various microscopic imaging techniques such as Raman spectroscopy, fluorescence microscopy, and laser direct infrared spectroscopy are used for particle identification [3] [11] [12] [10]. Although high-throughput filtration methods are effective for removing contaminants, a rapid microscopic free identification is needed to quickly test MNP contamination and overall water quality to determine if more advanced filtration is needed.

B. Scenario

In this scenario, we consider a plastic water bottle manufacturing plant that utilizes PET to produce plastic bottle lids. Routine operations result in MNP accumulation in the plant's wastewater. Simultaneously, an industrial process involving crude oil derivatives generates tiny oil droplets that end up in the same waste water as PET. This sensor's goal is to separate PET from the oil contaminants and measure the plastic's concentration based on particle size. We believe such a sensor would be broadly applicable to similar scenarios involving other types of contaminants, provided the sensors parameters are modified based on the specific contaminant or MNP targeted for separation and detection. This ideal and somewhat realistic scenario is designed to evaluate the effectiveness of a theoretical sensor by using a sample of distilled water (experiment dependent), MNPs (mean size of $1\ \mu\text{m} \pm 100\ \text{nm}$), and oil particles (mean size of $10 \pm 1\ \mu\text{m}$). In terms of concentrations, we acknowledge prior literature values (e.g., 2.0×10^3 fibers/L) as used by [4], but actual test concentrations should be experimentally determined for specific applications.

II. BACKGROUND INFORMATION

A. Microfluidics

Microfluidics allows for the separation, mixing, and reaction of substances on a miniaturized scale. These systems use channels ($1\ \mu\text{m}$ to $300\ \mu\text{m}$ wide) and reservoirs for manipulating matter. Within the past 20 years, the field of microfluidics has expanded to lab-on-chip devices, organ-on-chip, droplet microfluidic devices, optofluidics, and acoustofluidics [13].



Fig. 1: Workflow for the sensor: sample preparation, dilution, oil pollutant separation, microplastic concentration and separation, plastic detection, and data analysis.

The feasibility for microfluidics revolves around the unique physical laws for liquid in small quantities. At the micron scale, viscous forces dominate inertia which allows for fluids to travel through fabricated channels in laminar streams [13]. Ideal laminar flow indicates that the parallel fluid streams only mix by slowly molecular diffusion and remain largely "separated." Oftentimes, researchers will tune the Reynolds number (Re) by adjusting channel width, flow rate, microchannel material, and fluid viscosity [14]. Depending on whether laminar or turbulent flow is needed, a low Re is wanted for laminar behavior while higher Re is wanted for mixing. In our oil and microplastic separation device, laminar flow is preferred for the ability to maintain spatial control over each particle stream without major effects from motion or diffusion [13].

Ideally, constant pressure driven flow further minimizes any unwanted turbulence within the microchannels [4]. Additionally, channel dimensions are of significant influence in microfluidics. Typically, sub-millimeter channels limit volumetric throughput, but this is acceptable for our sensor as it is for the identification of particles rather than bulk filtration [12].

Microfluidic chips are usually fabricated with some combination of photolithography and etching on silicon, glass, or polymer substrates. The choice of substrate affects optical clarity, chemical compatibility, robustness, flexibility, acoustic impedance, etc. Polydimethylsiloxane (PDMS) remains popular for low cost prototyping despite the adhesion of molecules to its surface (depending on whether they are hydrophobic or hydrophilic) [13]. The surface adsorption described can be mediated with polymeric coatings such as polyethylene glycol (PEG), which reduces particle adhesion to the surfaces.

Ultimately, the proposed acoustofluidic separation of particles is a non-destructive technique that uses standing waves to manipulate suspended particles [9]. In our design, IDTs will generate standing waves that propagate through the channel walls and exert forces on the particles in the liquid for subsequent separation (basic process outlined in Figure 1). The microfluidic physics presented here are intentionally simplified, as the primary focus of this paper is for device fabrication rather than complete feasibility. We acknowledge the modeling assumptions and practical limitations, which will be examined in the discussion section.

B. Acoustophoresis

1) *Acoustophoretic Channel Fundamentals*: Acoustophoresis in microfluidic channels is used to isolate PET microparti-

cles from the solution. This process uses standing acoustic waves to create lateral pressure nodes in the direction of laminar fluid flow within a segment of the microfluidic channel [15] [16]. The density and size characteristics of the microparticles influence their response to the variable force by moving towards propagated wave nodes or antinodes, thus sorting material [17]. The figure (2) below depicts this movement.

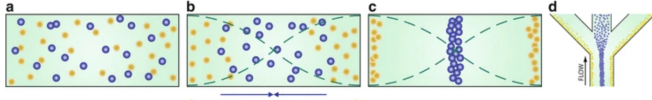


Fig. 2: Model of Acoustophoresis in Microfluidics, where blue particles concentrate on nodes, and yellow concentrate on anti-nodes [17].

To stimulate acoustic forces, a surface acoustic standing wave (SASW) topology is selected. This method, compared to the more common bulk acoustic standing wave (BASW) design, allows finer control of the induced forces within the fluidic channel [16] [18]. To produce SASWs, an alternating current (AC) voltage specific to the geometry of an interdigital electrode (IDT) and the cross-sectional geometry of the microfluidic channel is applied. The generated wavelength creates a standing wave with n nodes along the channel. The generated electric field by the IDT is absorbed by a piezoelectric substrate LiNbO_3 , where it expands and contracts to the applied field, thus generating a standing force against the solution within the chamber [16] [17].

The primary advantage of acoustophoresis is in its ability to separate particles by density, allowing an excellent and non-contact method of material dependent separation [19] [20]. The equation below characterizes the acoustic forces, where R , ρ , and β are radius, density, and compressibility respectively.

$$\mathbf{F}_{ac} = QU^2R^3 \varphi(\rho_p, \beta_p), \quad \varphi_p = \frac{5\rho_p - 2\rho_m}{2\rho_p + \rho_m} - \frac{\beta_p}{\beta_m} \quad (1)$$

From 1, the acoustic forces are cubed dependent on the radius of the particle and related to the particle's difference in density from the solution. The sign of the magnitude of \mathbf{F}_{ac} is determined by the density and compressibility comparison to the median solution [19].

Calculations of the contrast factor of PET and crude oil result in values of 0.55 and -1.337 respectively. This means the crude oil will respond with a force in the opposite magnitude of the PET. PET particles will gravitate towards standing wave pressure nodes, while crude oil will gravitate towards the anti-pressure nodes.

2) *Acoustophoretic Channel Design*: This sensor uses a cascade of acoustophoresis levels where the first stage primarily concentrates sorting particles by material (PET vs. crude oil). Since the magnitude of the force is proportional to the cubed radius of the particle, a longer 2nd stage is needed for the removal particles smaller than $1 \mu\text{m}$, where acoustic forces are not as dominant. Figure 3 depicts a transparent and top-down view of the core features for the design.

In the first stage particles are introduced from the sample collection reservoir to a $100 \mu\text{m}$ width microfluidic channel

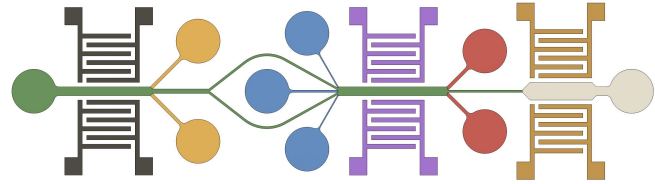


Fig. 3: Original conceptual layout of the multistage acoustophoretic-EIS microfluidic chip. A $100 \mu\text{m} \times 50 \mu\text{m}$ green inlet carries the mixed sample. Stage 1: black PZT IDTs generate a standing wave that deflects oil droplets into yellow outlet channels. Blue DI-water side inlets maintain continuous flow. Stage 2: purple PZT IDTs redirect nanoplastics toward the red collection channels and reservoirs, while larger microplastics proceed downstream. The tan chamber contains gold interdigitated electrodes for impedance spectroscopy of the isolated microplastics.

with an $n = 1$ standing acoustic 17.44 MHz wave. Details regarding the design choice of this frequency are covered in the following section. The acoustic wave applied induces a positive force on PET, moving it to align with the standing wave's pressure nodes, while the crude oil moves to the anti-nodes. The magnitude of this force is reduced for smaller particles, therefore the channel length is designed to be long enough for minimally $1 \mu\text{m}$ particles to align [20]. The combined output channels are $50 \mu\text{m}$ wide, accepting 50 percent of the initial sample volume.

In the second stage, microplastic particles are then sorted by size, where particles less than $1 \mu\text{m}$ are discarded. This is to prevent smaller non-plastic particles, dominated by Brownian motion from appearing in the sorted solution. Two $25 \mu\text{m}$ channels are inserted to a $100 \mu\text{m}$ channel, centered along 0.25 and 0.75 fractions of the width of the channel. This is such that the particles introduced are between the acoustic nodes and antinodes. Additionally, two $12.5 \mu\text{m}$ wide channels along the sides, and one $25 \mu\text{m}$ wide channel in the center introduce de-ozone water to ensure constant fluid volume per cross sectional area and laminar flow. The reservoir's colored in blue of figure 3 depict this design. The same $n = 1$ standing acoustic 17.44 MHz wave is introduced. The acoustic forces on the particles vary by the particle's size. Larger particles align quicker than smaller ones [21]. The acoustic channel for this chamber is designed such that only particles larger than $1 \mu\text{m}$ will have a strong enough acoustic force to align before the end of the chamber.

3) *Acoustophoretic IDT Design*: For proper wave propagation and uniform pressure nodes along the microfluidic channel, standing waves must travel along the surface of the piezoelectric surface towards the walls of the channel [15]. For best performance, inter-digital electrodes are designed as shown in Figure 4.

To generate a single-mode ($n = 1$) standing wave in a microfluidic channel of width $w = 100 \mu\text{m}$, we require the

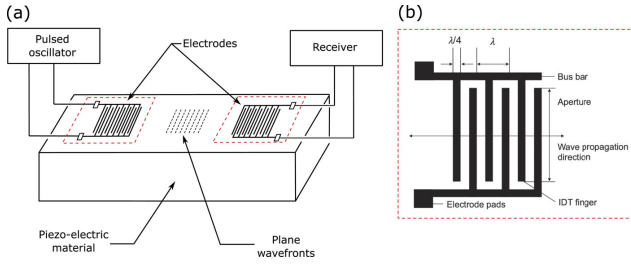


Fig. 4: SASW IDT geometry [15]

width to match half the acoustic wavelength:

$$w = \frac{\lambda}{2} \Rightarrow \lambda = 2w = 2 \times 100 \mu\text{m} = 200 \mu\text{m}$$

Given λ , the IDT is designed with by length to match Figure. 4.

The speed of sound in water is approximately:

$$v = 1500 \text{ m s}^{-1}$$

The resonant frequency is then:

$$f = \frac{v}{\lambda} = \frac{1500 \text{ m s}^{-1}}{200 \mu\text{m}} = \frac{1500}{200 \times 10^{-6}} = 7.5 \text{ MHz}$$

SAW Consideration on LiNbO₃: For a surface acoustic wave (SAW) propagating on a Y-cut, Z-propagating LiNbO₃ substrate, the SAW velocity is: [22] [20]

$$v_{\text{SAW}} \approx 3488 \text{ m s}^{-1}$$

To couple efficiently into a standing wave in the fluid with $\lambda = 200 \mu\text{m}$, the required IDT frequency is:

$$f_{\text{IDT}} = \frac{v_{\text{SAW}}}{\lambda} = \frac{3488}{200 \times 10^{-6}} = 17.44 \text{ MHz}$$

Ultimately, to form a single-mode standing wave across a $100 \mu\text{m}$ wide water-filled channel, the IDTs operate at approximately 17.44 MHz and $50 \mu\text{m}$ from the edge of the channel to launch a surface acoustic wave with wavelength $200 \mu\text{m}$.

C. EIS with Nanopatterned Electrodes

EIS is a label-free technique used to characterize the interfacial properties of electrochemical systems by applying a small-amplitude sinusoidal voltage and measuring the resulting current response over a wide frequency range. By analyzing the system's impedance as a function of frequency, EIS provides insight into charge transfer resistance, double-layer capacitance, diffusion processes, and dielectric properties within electrochemical cells. The presence of microplastics within the electrochemical cell disrupts ionic transport and alters the local dielectric environment, affecting measured impedance. EIS data is typically interpreted using equivalent circuit models (e.g., Randles circuit) or fitted empirically to extract parameters relevant to sensor performance, such as sensitivity and detection limits [23]. However, interpretation of EIS data can be subjective and model-dependent; recent studies have demonstrated the utility of machine learning approaches for more robust analysis and correlation with target analytes [24].

In this system, EIS is used after acoustophoretic sorting and focusing to detect and quantify separated PET microplastics. The EIS detection chamber functions as a two-electrode cell with reduced graphene oxide (rGO)-coated gold electrodes. The polar nature of rGO enhances electrochemical sensitivity to PET, a polar polymer, by supporting dielectric interactions. Additionally, the high effective surface area and electrical conductivity of rGO enhances PET detection by amplifying impedance changes associated with particle presence [25].

D. Support Vector Machines Interpretation of EIS

To improve the robustness of MNP detection, we will use support vector machines (SVMs) to classify impedance features from EIS spectra. This approach overcomes several limitations of traditional equivalent circuit modeling, which can be subjective and poorly suited for nonlinear systems. SVMs are particularly effective for small, high-dimensional datasets, allowing for the discrimination of subtle differences in impedance responses related to variations in MNP and oil droplet sizes and concentrations [26]. The SVM will be trained and developed as described in the methods section below.

III. MATERIALS AND METHODS FOR FABRICATION

The fabrication process of this sensor requires many conventional microfabrication techniques, such as photolithography, electron-beam (e-beam) evaporation, and liftoff. It also relies on soft lithography for microfluidic fabrication to streamline and simplify repetitive manufacturing. This section details the fabrication process of each component of this sensor. Wafer-scale fabrication enables multiple devices to be manufactured at once. A great amount of inspiration for this fabrication process was Marco Travaglini's microfluidic fabrication process [27].

A. Piezoelectric Transducer and EIS Electrodes

The fabrication of interdigitated transducers (IDTs) and EIS electrodes begins with a 128° Y-cut lithium niobate LiNbO₃ wafer, chosen for its piezoelectric properties that enable acoustophoretic manipulation.

The LiNbO₃ wafer is first cleaned by sequential sonication in acetone and 2-propanol for 10 minutes each, then dried using nitrogen gas. The nitrogen as opposed to other gases helps to prevent unnecessary oxidation. A dehydration bake at 115°C for 15 minutes follows to improve PR adhesion. Shipley S1818, a positive PR is spin coated at 4000 rpm for 1 minute to achieve a thickness of approximately $2 \mu\text{m}$ [27]. The coated wafer is then soft baked at 90°C for 1 minute. A darkfield photomask with IDT patterns, EIS electrode patterns, and electronic interconnects is aligned to the sample and exposed to UV light at an intensity of 55 mJ/cm^2 [27]. The sample is developed in Microposit MF319 developer for 1 minute, then immediately rinsed in DI water and dried with nitrogen gas to prevent overdevelopment. This is followed by a 5 minute hard bake at 115°C to remove residual moisture and improve metallization uniformity. Next, a 10 nm titanium adhesion layer is deposited using e-beam evaporation, followed by a 100 nm gold layer. Liftoff is then performed by sonicating the wafer in acetone for 15 minutes, followed

thorough rinsing with DI and drying with nitrogen gas. Wafers are then diced into individual sensor systems.

rGO is electrodeposited onto gold EIS electrodes from a 0.5 mg/mL graphene oxide solution (pH 4) by applying a cathodic potential of -1.0 V vs. Ag/AgCl for 300 seconds. This electrochemical reduction forms a thin, conductive rGO layer that enhances surface area and interfacial sensitivity for impedimetric MNP detection. This will be verified by performing EIS measurements of MNP suspensions with and without rGO-coated electrodes and comparing the relative sensitivity of the two electrode surfaces.

B. Microfluidics

Microfluidics are separately fabricated via soft lithography and bonded to patterned electrodes to streamline fabrication and enable modular system integration. First, a master mold of the channel layer is created. To do so, a silicon wafer is sequentially sonicated in acetone and 2-propanol for 10 minutes each, followed by drying with nitrogen gas. A dehydration bake is performed at 200°C for 10 minutes to ensure good adhesion of further patterning materials. SU-8 2050 (a negative PR) is selected as the mold material due to its inertness and rigidity for the target thickness of 50 μm . It is spin-coated at 3000 rpm until a 50 μm thickness is achieved. The PR is soft baked at 90°C for 1 minute on a hot plate. Next, it is exposed with an intensity of 175 mJ/cm². The non-exposed SU-8 is then developed using propylene glycol methyl ether acetate (PGMEA) for 5 minutes. The re-usability of this mold improves the efficiency of resource utilization and scalability of microfluidic fabrication. It also improves yield consistency for the large 50 μm fabricated fluidic channels.

To cast microfluidics using the mold, PDMS is first prepared by mixing Sylgard 184 Part A and B in a 10:1 ratio. It is then centrifuged for 2 min at 1320g for degassing. The PDMS is then slowly poured onto the master SU-8 mold in a petri dish to a total 1 mm height. The petri dish is placed in a vacuum chamber for 30 minutes to degas the PDMS further. The PDMS is then cured at 80°C for 1 hour. The solidified PDMS is then de-molded. Plasma treatment is then used to adhere the microfluidic device to the LiNbO₃ substrate.

C. SVM Development

To train the SVM, fluids containing known concentrations and sizes of MNPs and oil droplets will be injected into the sensing system and EIS measurements will be performed. EIS data will be labeled with concentrations and size distributions and used as model input. Cross-validation will be used to improve generalization and the SVM's performance will be assessed by injecting additional solutions with known particle concentrations and comparing predicted values to actual values.

IV. DISCUSSION

A. Microfluidics

The microfluidic channels are crucial in establishing an environment for highly effective acoustophoretic separation of PET from crude oil. Additionally, they must be capable of carrying a wide range of particles diameters, from 100 nm

to 10 μm . The microfluidic channels in this design minimally have a 1250 μm^2 cross-sectional area, allowing particles to flow freely with low risk of blockages. Variations in the concentration of particles along their flow may increase the risk of microfluidic blockages- although this risk is low. Additionally, undesirable particle adhesion to microfluidic walls reduce microfluidic area and EIS sensitivity. To further reduce the risk of the issues mentioned, our design could be modified by transitioning the plastic into another hydrophobic buffer with a higher viscosity. [21] Additionally, design would need to test fluid flow rate and pressure loss across the device to ensure proper laminar movement of the particles. [14]

In addition to the structural limitations of microfluidic channels, interference of acoustic waves between acoustophoretic stages also may reduce the effectiveness of this process. To best study these effects, different layouts involving dampening structures, such as reverse-polarity generated waves, or low dielectric constant blockage materials around the IDTs and microfluidic channels could be added.

B. Piezoelectric Transducer

The piezoelectric transducers, while ideal for wave SASW propagation, have limitations. First, the quality of wave propagation is based on how the material propagates the wave along the surface of the LiNbO₃ substrate. This propagation is improved with thinner IDTs, however, ultra thin films do not remain as stable under process, voltage, and temperature [28]. To compromise stability with quality of propagation, our design uses a 100 nm thick structure to improve stability. Additionally, standing wave creation is based on the intended number of standing nodes and path-length between the electrodes. This determines the resonating frequency. Some literature [21] suggests the overall net acoustic force is limited by the resonating frequency by particle size. To prove this, additional experimentation would be required to prove the frequency threshold would provide the net acoustic force required on the smaller particles. Variation in ambient temperature also change the IDT's resonant frequency and the LiNbO₃ substrate's response, reducing the total effectiveness of acoustophoresis [29]. Additional experiments on this device would be required to prove its effectiveness under these stresses.

C. EIS Detection

Given that EIS is highly sensitive to changes in fluid composition (e.g., ionic strength and pH), variations in the surrounding environment can lead to unpredictable fluctuations in impedance, complicating the interpretation of MNP-related signals. Additionally, the non-specific interactions of microplastics with electrode surfaces or the surrounding fluid may also introduce noise, further reducing the accuracy and reproducibility of the detection. As a result, control of fluid composition and advanced data processing techniques are necessary to improve the reliability of EIS-based MNP detection. These potential limitations may be reduced by using robust data for SVM training that accounts for variations in environmental conditions, enhancing the sensing system's ability to detect and quantify MNPs.

ABBREVIATIONS

Alternating Current, AC; Bulk Acoustic Standing Wave, BASW; Computer Aided Design, CAD; Electrochemical Impedance Spectroscopy, EIS; Electron-beam, E-beam; Interdigital Electrode, IDT; Micro- and Nanoplastic, MNP; Photoresist, PR; Polyamide, PA; Polydimethylsiloxane, PDMS; Polyethylene, PE; Polyethylene Glycol, PEG; Polyethylene Terephthalate, PET; Piezoelectric Transducer, PZT; Polypropylene, PP; Polystyrene, PS; Polyvinyl Chloride, PVC; Propylene Glycol Methyl Ether Acetate, PGMEA; Reduced Graphene Oxide, rGO; Reynolds Number, Re; Support Vector Machines, SVMs; Surface Acoustic Standing Wave, SASW;

AI USAGE STATEMENT

ChatGPT was used for deep research and textual editing with all content remaining original to the authors.

V. APPENDIX

https://github.com/jogoebel/Microplastic_Sensor.git

REFERENCES

- [1] M. Dokl, A. Copot, D. Krajnc, *et al.*, “Global projections of plastic use, end-of-life fate and potential changes in consumption, reduction, recycling and replacement with bioplastics to 2050,” *Sustainable Production and Consumption*, vol. 51, J. M. Ponce-Ortega, Ed., pp. 498–518, 2024. DOI: 10.1016/j.spc.2024.09.021. [Online]. Available: <https://www.sciencedirect.com/science/article/pii/S2352550924003087>.
- [2] N. Qian, X. Gao, X. Lang, *et al.*, “Rapid single-particle chemical imaging of nanoplastics by srs microscopy,” *Proceedings of the National Academy of Sciences of the United States of America*, vol. 121, no. 3, e2300582121, 2024, Epub 2024 Jan 8. DOI: 10.1073/pnas.2300582121.
- [3] H. Li, L. Zhu, M. Ma, H. Wu, L. An, and Z. Yang, “Occurrence of microplastics in commercially sold bottled water,” *Science of The Total Environment*, vol. 867, p. 161 553, 2023, ISSN: 0048-9697. DOI: 10.1016/j.scitotenv.2023.161553. [Online]. Available: <https://www.sciencedirect.com/science/article/pii/S0048969723001687>.
- [4] Y. Akiyama, T. Egawa, K. Koyano, and H. Moriwaki, “Acoustic focusing of microplastics in microchannels: A promising continuous collection approach,” *Sensors and Actuators B: Chemical*, vol. 304, p. 127 328, 2020, ISSN: 0925-4005. DOI: 10.1016/j.snb.2019.127328. [Online]. Available: <https://www.sciencedirect.com/science/article/pii/S0925400519315278>.
- [5] H. Wang, Z. Liu, S. Kim, *et al.*, “Microfluidic acoustophoretic force based low-concentration oil separation and detection from the environment,” *Lab on a Chip*, vol. 14, no. 5, pp. 947–956, 2014. DOI: 10.1039/C3LC51032H.
- [6] F. Wang, Q. Meng, C. Lin, X. Wang, and W. Weng, “Study of oil particle concentration vertical distribution of various sizes under displacement ventilation system in large-space machining workshop,” *International Journal of Environmental Research and Public Health*, vol. 19, no. 11, p. 6932, 2022. DOI: 10.3390/ijerph19116932.
- [7] Y. Yu, Z. Qi, D. Xiong, R. Sun, S. Fu, and W. Li, “Oil dispersion and aggregation with suspended particles in a wave tank,” *Journal of Environmental Management*, vol. 278, no. Part 2, p. 111 572, 2021, ISSN: 0301-4797. DOI: 10.1016/j.jenvman.2020.111572. [Online]. Available: <https://www.sciencedirect.com/science/article/pii/S0301479720314973>.
- [8] A. D. M. d. Medeiros, C. J. G. d. Silva Junior, J. D. P. d. Amorim, I. J. B. Durval, A. F. d. S. Costa, and L. A. Sarubbo, “Oily wastewater treatment: Methods, challenges, and trends,” *Processes*, vol. 10, no. 4, 2022, ISSN: 2227-9717. DOI: 10.3390/pr10040743. [Online]. Available: <https://www.mdpi.com/2227-9717/10/4/743>.
- [9] T. Klymkovych, N. Bokla, O. Matviyukiv, and V. Stakhiv, “Simulation and analysis of microparticles acoustophoretic separation in multi-channel lab-chip device,” in *2021 IEEE 16th International Conference on the Experience of Designing and Application of CAD Systems (CADSM)*, Lviv, Ukraine: IEEE, 2021, pp. 29–33. DOI: 10.1109/CADSM52681.2021.9385236.
- [10] M. Rani, S. Ducoli, L. E. Depero, *et al.*, “A complete guide to extraction methods of microplastics from complex environmental matrices,” *Molecules*, vol. 28, no. 15, Y. Yang, Ed., p. 5710, 2023. DOI: 10.3390/molecules28155710.
- [11] M. S.-L. Yee, L.-W. Hii, C. K. Looi, *et al.*, “Impact of microplastics and nanoplastics on human health,” *Nanomaterials*, vol. 11, no. 2, p. 496, 2021. DOI: 10.3390/nano11020496.
- [12] A. de Hemptinne, V. R. Misko, P. Gelin, and W. D. Malsche, “Acoustic standing wave with a frequency sweeping in a microfluidic system of parallel channels,” *Chemical Engineering and Processing - Process Intensification*, vol. 194, p. 109 607, 2023, ISSN: 0255-2701. DOI: 10.1016/j.cep.2023.109607. [Online]. Available: <https://www.sciencedirect.com/science/article/pii/S0255270123003446>.
- [13] N. L. Perera, “Acoustofluidics for the removal of microplastics and the detection of viruses,” Ph.D. Dissertation, New Mexico Institute of Mining and Technology, Socorro, New Mexico, Jul. 2023.
- [14] L. N. Perera and M. E. Piyasena, “Acoustic focusing of microplastics in microfabricated and steel tube devices: An experimental study on the effects from particle size and medium density,” *Separation and Purification Technology*, vol. 288, p. 120 649, 2022, ISSN: 1383-5866. DOI: 10.1016/j.seppur.2022.120649. [Online]. Available: <https://www.sciencedirect.com/science/article/pii/S138358662200209X>.
- [15] L. T. Lenshof A., “Acoustophoresis,” *Bhushan, B. (eds) Encyclopedia of Nanotechnology*, 2012, ISSN: 978-90-

- 481-9751-4. DOI: https://doi.org/10.1007/978-90-481-9751-4_423. [Online]. Available: <https://www.sciencedirect.com/science/article/pii/S0301479720314973>.
- [16] Y. Zhou, "Comparison of numerical models for bulk and surface acoustic wave-induced acoustophoresis in a microchannel," *The European Physical Journal Plus*, vol. 135, no. 9, p. 696, 2020. DOI: 10.1140/epjp/s13360-020-00697-x.
- [17] M. S. Namnabat, M. Moghimi Zand, and E. Houshfar, "3d numerical simulation of acoustophoretic motion induced by boundary-driven acoustic streaming in standing surface acoustic wave microfluidics," *Scientific Reports*, vol. 11, no. 1, p. 13 326, 2021. DOI: 10.1038/s41598-021-90825-z.
- [18] A. Lenshof, C. Magnusson, and T. Laurell, "Acoustofluidics 8: Applications of acoustophoresis in continuous flow microsystems," *Lab on a Chip*, vol. 12, no. 7, pp. 1210–1223, 2012. DOI: 10.1039/C2LC21256K.
- [19] V. Bogatyr, A. S. Biebricher, G. Bergamaschi, E. J. G. Peterman, and G. J. L. Wuite, "Quantitative acoustophoresis," *ACS Nanoscience Au*, vol. 2, no. 4, pp. 341–354, 2022. DOI: 10.1021/acsnanoscienceau.2c00002. [Online]. Available: <https://doi.org/10.1021/acsnanoscienceau.2c00002>.
- [20] S. K. Sankaranarayanan and V. R. Bhethanabotla, "Numerical analysis of wave generation and propagation in a focused surface acoustic wave device for potential microfluidics applications," *IEEE Transactions on Ultrasonics, Ferroelectrics, and Frequency Control*, vol. 56, no. 3, pp. 631–643, 2009. DOI: 10.1109/TUFFC.2009.1079.
- [21] M. Wu, A. Ozcelik, J. Rufo, Z. Wang, R. Fang, and T. J. Huang, "Acoustofluidic separation of cells and particles," *Microsystems & Nanoengineering*, vol. 5, no. 1, p. 32, 2019. DOI: 10.1038/s41378-019-0064-3. [Online]. Available: <https://www.nature.com/articles/s41378-019-0064-3>.
- [22] T. D. Luong and N.-T. Nguyen, "Surface acoustic wave driven microfluidics – a review," *Micro and Nanosystems*, vol. 2, no. 3, pp. 217–225, 2010. DOI: 10.2174/1876402911002030217. [Online]. Available: https://www.researchgate.net/publication/230852272_Surface_Acoustic_Wave_Driven_Microfluidics_-_A_Review.
- [23] A. Lasia, "Electrochemical impedance spectroscopy and its applications," in *Modern Aspects of Electrochemistry*, B. E. Conway, J. O. Bockris, and R. E. White, Eds. Boston, MA: Springer US, 2002, ISBN: 978-0-306-46916-9. DOI: 10.1007/0-306-46916-2_2.
- [24] V. Bongiorno, S. Gibbon, E. Michailidou, and M. Curioni, "Exploring the use of machine learning for interpreting electrochemical impedance spectroscopy data: Evaluation of the training dataset size," *Corrosion Science*, vol. 198, p. 110 119, 2022, ISSN: 0010-938X. DOI: <https://doi.org/10.1016/j.corsci.2022.110119>.
- [25] H. Du, G. Chen, and J. Wang, "Highly selective electrochemical impedance spectroscopy-based graphene electrode for rapid detection of microplastics," *Science of The Total Environment*, vol. 862, p. 160 873, 2023, ISSN: 0048-9697. DOI: <https://doi.org/10.1016/j.scitotenv.2022.160873>. [Online]. Available: <https://www.sciencedirect.com/science/article/pii/S0048969722079761>.
- [26] V. Meiler, J. Pfeiffer, L. Bifano, C. Kandlbinder-Paret, and G. Fischerauer, "Approaches to detect microplastics in water using electrical impedance measurements and support vector machines," *IEEE Sensors*, vol. 23, no. 5, pp. 4863–4872, 2023. DOI: 10.1109/JSEN.2023.3236375.
- [27] M. Travagliati, R. Shilton, F. Beltram, and M. Cecchini, "Fabrication, operation and flow visualization in surface-acoustic-wave-driven acoustic-counterflow microfluidics," *Journal of Visualized Experiments*, vol. 78, p. 50 524, 2013. DOI: 10.3791/50524. [Online]. Available: <https://www.jove.com/v/50524/fabrication-operation-flow-visualization-surface-acoustic-wave-driven>.
- [28] S. Song, Q. Wang, J. Zhou, and A. Riaud, "Design of interdigitated transducers for acoustofluidic applications," *Nanotechnology and Precision Engineering*, vol. 5, no. 3, p. 035 001, 2022. DOI: 10.1063/1.50013405. [Online]. Available: <https://pubs.aip.org/tu/npe/article/5/3/035001/2845629/Design-of-interdigitated-transducers-for>.
- [29] Z. Zhou, H. Wang, and L. Lou, "Design and characterization of surface acoustic wave-based wireless and passive temperature sensing system," *Micromachines*, vol. 15, no. 4, p. 544, 2024. DOI: 10.3390/mi15040544. [Online]. Available: <https://www.mdpi.com/2072-666X/15/4/544>.